Journal of Applied Physics

Nanoindentation applied to ion-irradiated and neutron-irradiated Fe-9Cr and Fe-9Cr-NiSiP model alloys

Cite as: J. Appl. Phys. **132**, 045101 (2022); https://doi.org/10.1063/5.0098807
Submitted: 12 May 2022 • Accepted: 04 July 2022 • Published Online: 22 July 2022

Frank Bergner, Cornelia Kaden, Aniruddh Das, et al.

Journal of Applied Physics METHOD scitation.org/journal/jap

Nanoindentation applied to ion-irradiated and neutron-irradiated Fe-9Cr and Fe-9Cr-NiSiP model alloys

Cite as: J. Appl. Phys. **132**, 045101 (2022); doi: 10.1063/5.0098807
Submitted: 12 May 2022 · Accepted: 4 July 2022 ·
Published Online: 22 July 2022

Frank Bergner,[1,a)] Cornelia Kaden,[1] Aniruddh Das,[1] Susana Merino,[2] Gonzalo Diego,[2] and Peter Hähner[3]

AFFILIATIONS

[1]Helmholtz-Zentrum Dresden-Rossendorf (HZDR), Bautzner Landstr. 400, 01328 Dresden, Germany
[2]Centro de Investigaciones Energéticas, Medioambientales y Tecnológicas (CIEMAT), Avda. Complutense 40, 28040 Madrid, Spain
[3]European Commission, DG Joint Research Centre, Nuclear Safety and Security Directorate, Westerduinweg 3, 1755 LE Petten, The Netherlands

Note: This paper is part of the Special Topic on Radiation Effects in Materials.
[a)]**Author to whom correspondence should be addressed:** f.bergner@hzdr.de. **Tel.:** +49 351 260 3186.

ABSTRACT

Nanoindentation of ion-irradiated materials has attracted much interest as a tool envisaged to derive the dose dependence of bulk-equivalent hardness from small samples. A major challenge arises from the steep damage gradient in the thin ion-irradiated layer and its unavoidable interplay with the indentation size effect. The present study relies on a number of choices aimed at simplifying the interpretation of the results and strengthening the conclusions. The studied alloys are two ferritic Fe-9Cr model alloys differing in controlled amounts of Ni, Si, and P known to enhance irradiation hardening. Both ion-irradiated (5 MeV Fe^{2+} ions) and neutron-irradiated samples along with the unirradiated references were investigated using Berkovich tips. According to the collaborative nature of the study, tests were conducted in two different laboratories using different equipment. A generalized Nix–Gao approach was applied to derive the bulk-equivalent hardness and characteristic length scale parameters for the homogeneous unirradiated and neutron-irradiated samples. Comparison with Vickers hardness indicates a 6% overestimation of the bulk-equivalent hardness as compared to the ideal correlation. For the case of ion irradiation, a first model assumes a homogeneous irradiated layer on a homogeneous substrate, while a second model explicitly takes into account the damage gradient. The first model was combined with both the original and the generalized Nix–Gao relation. We have found that the results revealed for Fe-9Cr vs Fe-9Cr-NiSiP are compatible with expectations based upon known irradiation-induced microstructures. The bulk-equivalent hardness derived for ion-irradiated samples reasonably agrees with the observation for neutron-irradiated samples.

I. INTRODUCTION

The first interest in using heavy ion irradiations to investigate neutron irradiation damage in materials dates back to the 1970s.[1] This interest has increased considerably since because of a combination of factors: a growing need to understand irradiation effects on nuclear materials under a variety of fission- or fusion-relevant conditions along with limited access to neutron irradiation facilities and limited variability of irradiation parameters. This prompted studies on issues that need to be addressed when attempting to transfer results obtained for ion-irradiated materials to the case of neutron environments.[2] These issues include the effect of implanted ions and the vicinity of a surface,[3–5] the effect of higher dose rates,[3,6] effects related to the energy spectrum and cascade morphology,[3] scanning beam vs defocused beam[7] and pulsed vs continuous irradiation,[8] the angle of incidence of the ion beam,[9] and carbon contamination.[10,11] Most noteworthy, these studies indicate that ion energies larger than 5 MeV, depending on the irradiation temperature, have to be used in order for a "safe zone"[3] with respect to ion–neutron transferability to be formed.

Depth-sensing nanoindentation of materials using pointed indenter tips and suitable contact stiffness recording allows the

indentation hardness to be derived as a function of contact depth in the range from less than 0.1 μm to more than 1 μm.[12–14] The combination of ion irradiation with nanoindentation is a powerful tool for the characterization of irradiation effects on nuclear materials,[15–19] e.g., Fe–Cr-based alloys.[20–27] Advantages are economy in terms of experiment time, sample volume, and avoidance of material activation.[2] Each of these advantages has counterparts that manifest themselves in ion–neutron and/or nano–macro transferability issues. For ion-irradiated layers to be efficiently probed, the depth of penetration of the indenter tip necessarily has to be small, of the order of 100 nm, resulting in interference of the indentation size effect[28,29] (ISE) with the irradiation effect. Approaches to handle this interference have been suggested[17,18,25,30–32] and related issues have been reviewed.[33–37] A simplified, but particularly clear, approach[18] is based on the following assumptions and approximations: (i) a rectangular damage profile, i.e., a homogeneous layer on a homogeneous substrate,[18] (ii) a hemispherical plastic zone,[38] (iii) the interpretation of the measured hardness as the weighted average of the layer hardness and the substrate hardness with the volume fractions of the plastic zone occupied by layer and substrate taken as weights,[34,38] and (iv) the consideration of the ISE for both layer and substrate according to the original Nix–Gao law.[28] This approach will be taken as starting point for the ion-irradiated samples of the present study. Major issues are the proper consideration of the damage gradient in the irradiated layer[31,32,39,40] and the breakdown of the Nix–Gao law at small indentation depth.[41–45] Other factors including the shape of the plastic zone,[46] the superposition of hardness contributions,[47] and the effect of implanted ions[40] will not be explicitly addressed in the present study.

The breakdown of the Nix–Gao law was demonstrated to be at least partly due to a maximum allowable density of geometrically necessary dislocations (GNDs) beneath the indenter instead of an unbounded increase of this density for decreasing indentation depths.[41–45] This was shown for homogeneous (e.g., unirradiated or neutron-irradiated) samples, but it should also be essential for appropriate analysis of nanoindentation results obtained for ion-irradiated samples. Another limitation of the simplified approach[18] mentioned above is the assumption of a rectangular damage profile. The real damage profile, typically approximated by means of the binary collision code SRIM,[48] may strongly deviate from this idealization, in particular, for self-ion irradiations using single ion energy. Reported work dedicated to this issue assumed the depth-dependent hardening (or defect density[39]) to be a linear,[39] square-root,[32] or power-law function[25,31] of displacement damage.

Comparably few direct applications of nanoindentation to neutron-irradiated samples have been reported.[19,23,24,49,50–53] However, application of essentially the same procedures of nanoindentation testing and analysis to unirradiated, ion-irradiated, and neutron-irradiated samples may reduce uncertainties as compared to conversions between as-measured nanoscale and reported macroscale properties.

Here, we applied nanoindentation on samples of two Fe-9Cr-based model alloys exposed to irradiation with either Fe^{2+} ions of 5 MeV energy or neutrons along with the unirradiated reference samples. The second alloy mainly differs from the first with respect to the addition of controlled amounts of Ni, Si, and P, which give rise to minor differences in the microstructures and mechanical properties of the pristine materials but pronounced differences in irradiation hardening. The irradiated microstructures of both alloys are known from reported studies.[54–57] Sample preparation and nanoindentation testing were performed in two laboratories according to slightly different but qualified procedures, which forms a basis to rationalize the effect of systematic errors in addition to statistical errors from repeated tests. The experimental work and related modeling were part of the collaborative European project M4F.[58] For the homogeneous unirradiated or neutron-irradiated samples, the original as well as a generalized Nix–Gao approach were applied to fit indentation hardness as a function of contact depth and extract related model parameters. For the ion-irradiated samples, the intrinsic hardening in the irradiated layer was modeled either as an effective rectangular profile or as a power-law function of the displacement damage obtained by SRIM calculations. The first option was combined with both the original and generalized Nix–Gao equation. We critically compared different model versions for ion-irradiated materials, bulk-equivalent hardness with Vickers hardness for both unirradiated and neutron-irradiated materials, as well as ion-induced with neutron-induced hardness changes.

TABLE I. Composition (analysis) in weight %.

Alloy	Code	C	N	Si	P	Cr	Ni
Fe-9Cr	G385	<0.006	<0.005	0.004	0.003	9.1	0.009
Fe-9Cr-NiSiP	G389	<0.006	<0.005	0.221	0.032	9.1	0.092

II. EXPERIMENTS

A. Materials and samples

Fe-9Cr-type model alloys of high purity were cast and hot rolled at OCAS (Gent, Belgium) as part of a larger program. The compositions are summarized in Table I. A detailed account of the impurity limits as well as the thermal and mechanical history of the materials can be found elsewhere.[59] The microstructure is essentially ferritic. Grain size, dislocation density, and measured mechanical properties are specified in Table II.

Samples of size $10 \times 10 \times 1$ mm^3 (for ion irradiation) or diameter 9×1 mm^2 (for neutron irradiation) were machined from the delivered plates. The sample surfaces were prepared before irradiation for the ion-irradiated samples but after irradiation for the neutron-irradiated samples. After stepwise grinding and mechanical polishing, several validated procedures of electrolytic polishing (labeled E, E1, and E2) were applied according to the best practice of the contributing laboratories.[60–62] At CIEMAT, disks (intended

TABLE II. Microstructure parameters and mechanical properties.

Alloy	Grain size (μm)	Dislocation density (10^{13} m^{-2})	Yield stress (MPa)	Vickers hardness HV10
Fe-9Cr	24.7	1.62[55]	252	117
Fe-9Cr-NiSiP	27.3	1.39[55]	257	115

for TEM) of 3 mm diameter and approximately 0.3 mm thickness were punched out from the neutron-irradiated samples and exposed to mechanical polishing followed by electrolytic polishing (procedure E2). At HZDR, electrolytic polishing was not possible for neutron-irradiated samples. Therefore, mechanical grinding up to paper P4000 and mechanical polishing (labeled M) was applied using 1 μm "MetaDi" diamond suspension (force 20 N, 150 rpm) as the last step. Line profiles at the mm length scale using a stylus-type instrument indicated roughness values R_a of approximately 15 and 20 nm for procedures E and M, respectively. The consistency of the results obtained for different surface preparation procedures was checked for special cases in the present study (see below). It is important to emphasize that the unirradiated reference samples were always prepared according to the same procedure as the respective irradiated samples.

B. Irradiations

All ion irradiations were carried out at the 3 MV tandetron accelerator facility of the Ion Beam Center located at HZDR, Dresden. Fe^{2+} ions of 5 MeV energy were implanted by x/y raster scanning the ion beam on the polished sides of the samples. The horizontal and vertical frequency of scanning was 1041 and 1015 Hz, respectively, allowing laterally uniform irradiation to be achieved. The irradiation temperature measured at the back side of the samples was 300 °C, the total ion fluence was 2.4×10^{15} cm^{-2}, and the irradiation time was 11 700 s. Several measures,[58] including plasma cleaning of the samples and maintenance of a high vacuum of the order of 10^{-5} Pa in the irradiation chamber, were taken to minimize carbon contamination during the ion irradiations. Both "1 dpa" and "0.1 dpa" (displacements per atom) irradiations were covered in the study. The full depth profiles of displacement damage and the concentration of implanted Fe ions calculated using the binary collision code SRIM[48] according to reported recommendations[63] (quick calculation mode, lattice binding energy and surface binding energy set to zero, displacement energy 40 eV) are shown in Fig. 1 for the "1 dpa" irradiations. For the "0.1 dpa" irradiation, divide vertical axes by 10. The dashed line indicates an average box-like dpa profile, required for modeling, with an average value of 1.36 dpa and an equivalent depth of 1.65 μm.

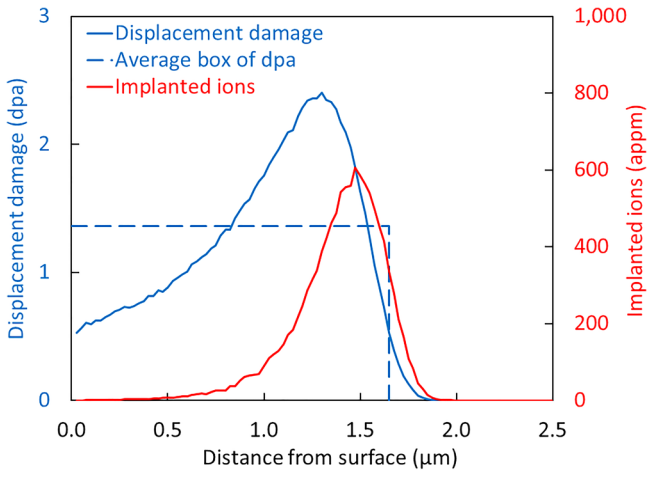

FIG. 1. Profiles of displacement damage and implanted ions for the "1 dpa" irradiations. Divide vertical axes by 10 for the "0.1 dpa" irradiation. The dashed line indicates an average box-like dpa profile.

Neutron irradiation was performed in the BR2 materials testing reactor of SCK CEN.[59] The irradiation temperature of 290 °C was guaranteed by the temperature of the flowing water. The neutron flux was 1.5×10^{13} cm^{-2} s^{-1} ($E > 1$ MeV). Dosimetry indicated total displacement damage of 0.11 dpa.

C. Methods

For room-temperature nanoindentation tests at CIEMAT (hereafter referred to as Lab 1), an MTS NANO-Indenter XP with nanopositioning stage and continuous stiffness measurement (CSM) functionality were used. The tip area function of the Berkovich indenter was calibrated using a fused quartz standard of known mechanical properties. Indents were set in arrays of 7×7 and 5×5 with 50 μm separation distance between adjacent indents. The CSM mode (harmonic displacement amplitude 2 nm, frequency 40 Hz) was applied with displacement control over 2000 nm and segments were needed for surface detection, creep correction, and thermal drift correction. Using the software for the CSM mode, zero-point determination was based on the dependence of harmonic stiffness on displacement. The zero-point was visually checked and, if necessary, corrected for each indentation individually. The recently reported[64] method of zero-point correction has not been applied. This point will be addressed in Sects. III and IV. Selection between all values of each array was carried out automatically and/or manually excluding individual indentations by applying criteria based on microstructural characteristics, corrupted surface detections, or outliers. The collection of datasets was formed on approximately 15–30 indentations depending on the selected criteria. Indentation hardness H_{IT}, reduced modulus E_r, and contact depth h_c with their standard deviations were calculated according to the Oliver–Pharr method.[12]

At HZDR (hereafter referred to as Lab 2), room-temperature nanoindentation was conducted in closed-loop load control using a Universal Nanomechanical Tester (UNAT, ASMEC GmbH) equipped with a Berkovich diamond indenter. The area function of the indenter and the system stiffness were calibrated by way of measurements on fused silica and sapphire with known bulk moduli. Indents were set in arrays of 4×10 with 40 μm separation distance between adjacent indents. The maximum load was 50 mN. For tentative piezo-based surface detection, a "surface approach" segment (threshold force 40 μN, lowest speed of approach 0.3 μm/s) was included in the test cycle. After testing, the zero-point was corrected for each individual indentation by fitting an expression based on the Hertzian contact theory to the data and extrapolating it down to zero. Using the supplied software, the fit range was manually modified until the best fit was achieved. The typical statistical error of zero-point determination was 1 nm. The quasi-continuous stiffness measurement (QCSM) mode was applied in order to determine the contact stiffness and calculate the contact depth according to the Oliver–Pharr method.[12] At 75 discrete load levels,

the load increase was paused for 3 s while overlaid by a sinusoidal oscillation of a frequency of 8.494 Hz and an amplitude of 0.3 V. Segments at maximum load (20 s duration) and 5 mN (60 s duration) were introduced for the purpose of creep and thermal drift corrections, respectively. The indentation hardness H_{IT} was calculated as a function of the contact depth from approximately 30 indentation tests by averaging after manually excluding occasional outliers.

The software supplied by the manufacturers of the nanoindentation devices was used to obtain records of contact depth, indentation hardness, reduced modulus, and indentation modulus with standard deviations and/or mean errors of the mean values. The latter type of errors is indicated in the plots of the present study. No additional corrections were carried out. In fact, radial displacement correction[13,65] was found to be negligible. An atomic force microscope (AFM) aimed at deriving pileup corrections[36] was not available for the present study, in particular, not for the neutron-irradiated samples. Pileup corrections were reported to be essential in terms of absolute hardness.[36,66] The irradiation-induced change of the pileup behavior was also addressed. To be more specific, these authors[66] observed an increase of the pileup height for a Berkovich-indentation depth of 250 nm from approximately 30 nm for the unirradiated reference to 50 nm for Fe-12Cr ion-irradiated up to 6.18 dpa (that is Σ5 times more than the present irradiation). Reported results[36] will serve as a basis to consider related systematic errors in the discussion. Finally, elastic modulus based pileup correction,[24,60] which does not require AFM measurements, was checked but found to cause unreasonable bias among a wider range of materials and ion energies in the present case.

The Vickers hardness HV10 (load 98.1 N) was measured for unirradiated and neutron-irradiated samples by averaging over ten tests for each sample.

III. RESULTS

A. Comparison of procedures

Typical results of the indentation modulus E_{IT} as a function of contact depth h_c are plotted in Fig. 2. Ideally, the indentation modulus should be independent of both contact depth and, for the present range of displacement damage, irradiation. However, our measurements indicate a trend for the modulus to increase from (215 ± 15) GPa at larger depths to (245 ± 15) GPa at smaller depths. Moreover, we have observed irradiation-induced increases of the modulus, which are limited to smaller depths for ion irradiation but extend toward the largest depths for neutron irradiations. These findings suggest indentation pileup being the major source of modulus variation in the present case (see Sec. IV). However, we cannot exclude minor issues due to recently reported limitations related to the applied methods of zero-point determination[64] and area-function calibration.[67]

Prior to a systematic presentation of the complete set of nanoindentation results, it is important to compare results obtained using different equipment or different surface preparation procedures. The indentation hardness H_{IT} as a function of contact depth h_c is plotted in Fig. 3(a) for unirradiated samples of Fe-9Cr. A wider range of the contact depth was covered in Lab 1. The results obtained in Lab 1 for surface preparation procedures E1 and E2,

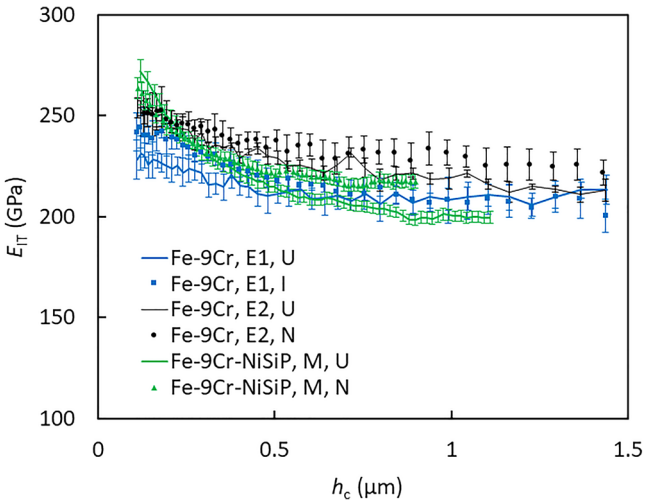

FIG. 2. Measured indentation modulus plotted as a function of contact depth for samples of Fe-9Cr and Fe-9Cr-NiSiP. Surface preparation procedures (E1, E2, and M, see above) and irradiation conditions (U = unirradiated reference, I = "0.1 dpa" ion irradiation, N = 0.11 dpa neutron irradiation) are indicated.

which were used as a reference for ion-irradiated and neutron-irradiated samples, respectively, exhibit minor but significant differences. Generally speaking, the measured differences must be due to differences between the experimental procedures. The most obvious ones are related to surface preparation (E1 vs E2) and the sample size ($10 \times 10 \times 1$ mm^3 vs disks of 3 mm diameter × 0.3 mm thickness). We have also observed significant differences between the unirradiated samples tested in Labs 1 and 2, which may be due to one or more of the following factors: surface preparation procedure (E1/E2 vs E), indenter tip (both are Berkovich tips with independently optimized area functions), and test procedure (e.g., CSM vs QCSM, see above). However, it is important to note that the ion-irradiation-induced hardness differences obtained in Labs 1 and 2 agree within the error, see Fig. 3(b). Indeed, both difference curves indicate significant irradiation-induced hardness increases throughout the covered range exhibiting a peak at approximately the same contact depth of 0.25 μm.

A comparison of results obtained for electrolytically (E) and mechanically (M) polished unirradiated Fe-9Cr-NiSiP is shown in Fig. 4 with a repeated measurement (U2) included. These samples were taken as references for ion-irradiated and neutron-irradiated samples, respectively. The curves agree within error margins for contact depths greater than 0.1 μm, but E and M diverge below 0.1 μm. The almost perfect agreement may be coincidental as both Berkovich indenter (B4 vs B5, both with individually optimized area functions) and surface preparation procedure (E vs M) were changed simultaneously for technical reasons. In any case, the unirradiated samples serve as suitable references for the ion-irradiated (E) and neutron-irradiated (M) samples, the latter limited to $h_c > 0.1$ μm.

In summary, the differences between Labs 1 and 2 and between different surface preparation procedures are reasonable

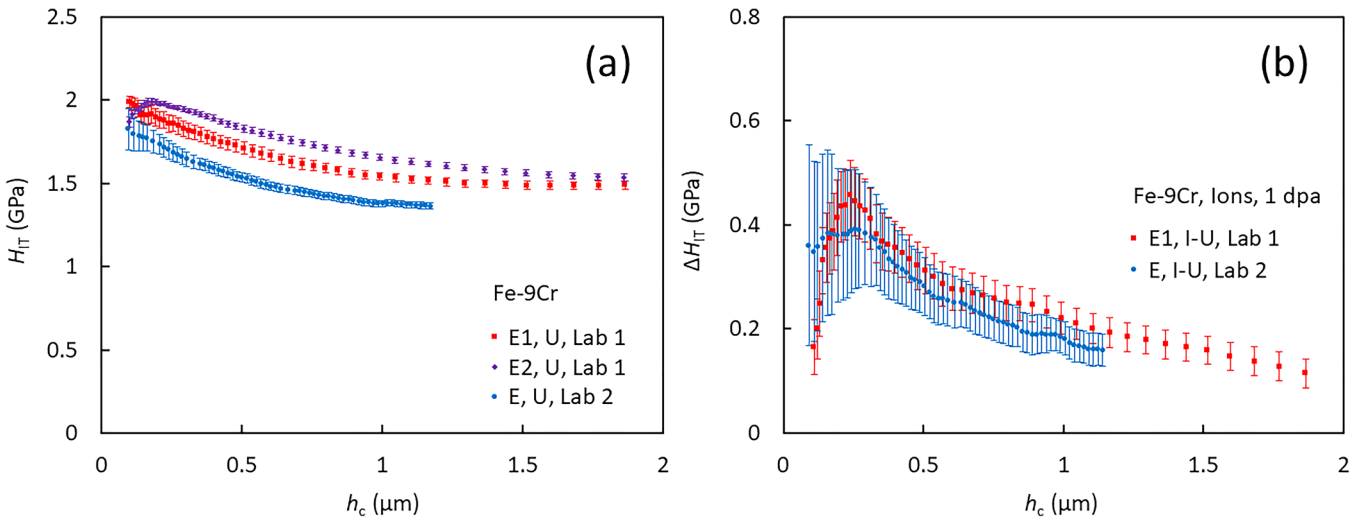

FIG. 3. (a) Average H_{IT}–h_c curves measured in Labs 1 and 2 for unirradiated Fe-9Cr; (b) average ion-irradiation-induced (1 dpa) hardness differences obtained in Labs 1 and 2.

and well within the interlaboratory scatter observed in a Round Robin, within which the same surface preparation procedure was applied for all labs.[60] Hence, both sets of data can be discussed consistently in a common framework.

B. Irradiated samples

Figure 5 summarizes the average H_{IT}—h_c curves measured for the ion-irradiated samples. The results obtained for ion-irradiated Fe-9Cr and Fe-9Cr-NiSiP (labeled I) are shown in Figs. 5(a) and 5(c) along with the unirradiated references (labeled U). Figures 5(b) and 5(d) represent the same data in terms of the irradiation-induced increase of hardness (labeled I-U). We have found that the unirradiated indentation hardness of Fe-9Cr-NiSiP is slightly higher than the hardness of Fe-9Cr and that the irradiation-induced increase of the former is higher by more than a factor 2 than the increase of the latter. The average ΔH_{IT}—h_c curves tend to form peaks at finite contact depths in the range between 0.15 and 0.3 μm. The irradiation-induced hardness increase for the "1 dpa" irradiation is higher, approximately twice as high as that for the "0.1 dpa" irradiation.

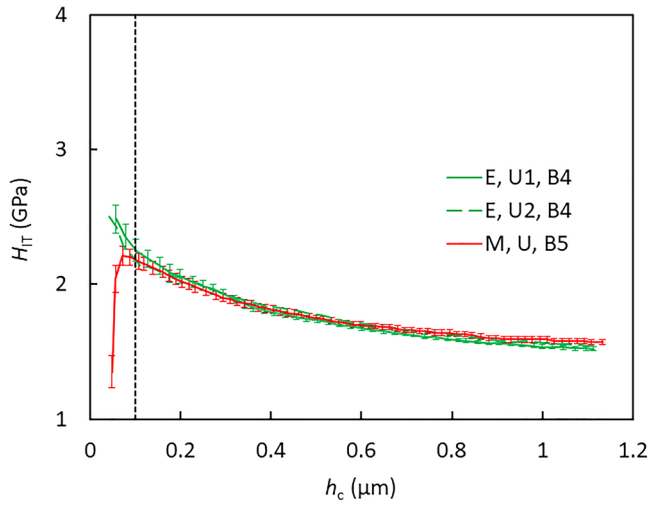

FIG. 4. Comparison of average H_{IT}–h_c curves measured for electrolytically and mechanically polished samples of unirradiated Fe-9Cr-NiSiP.

Figure 6 summarizes the average H_{IT}–h_c curves measured for the neutron-irradiated samples. Figure 6(a) shows the results of nanoindentation tests for electro-polished samples (procedure E2, TEM-type samples) neutron-irradiated Fe-9Cr (labeled N) along with the unirradiated reference (labeled U). The effect of neutron irradiation on mechanically polished (label M) samples of Fe-9Cr-NiSiP is indicated in Fig. 6(b). A comparison with results for ion-irradiated Fe-9Cr-NiSiP is included in Fig. 6(b). Both materials exhibit a neutron-irradiation-induced hardness increase revealing a weak dependence on the contact depth.

C. Generalized Nix–Gao analysis

In order to rationalize the indentation size effect (ISE) for homogeneous samples, Nix and Gao[28] introduced an approach based on the concept of geometrically necessary dislocations (GNDs), Eq. (1). It proceeds on the assumption that GNDs (accounting for the geometrical shape of an indent and associated strain gradients) come on top of the statistically stored dislocations (redundant carriers of plastic deformation in the absence of a strain gradient) and, hence, induce an additional hardness

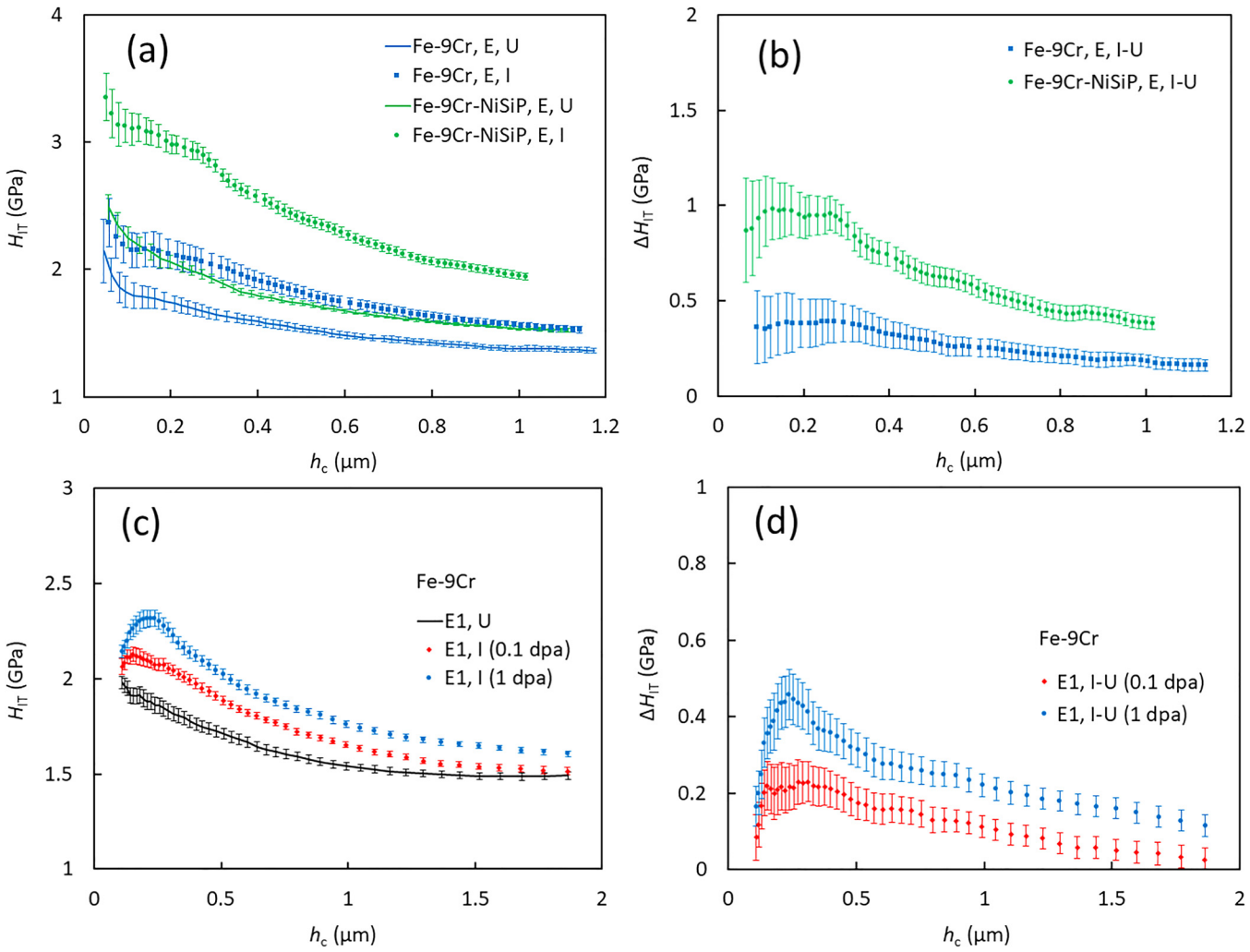

FIG. 5. Results of nanoindentation tests for ion-irradiated samples. (a) "1 dpa" ion irradiations of Fe-9Cr and Fe-9Cr-NiSiP along with unirradiated references; (b) corresponding irradiation-induced hardness increases; (c) "0.1 dpa" and "1 dpa" ion irradiations of Fe-9Cr along with unirradiated reference; (d) corresponding irradiation-induced increases.

contribution

$$H_{IT} = H_0\sqrt{1+\frac{h^*}{h_c}}. \quad (1)$$

The parameters can be interpreted as the bulk-equivalent hardness H_0, which accounts for the self-similar (i.e., indentation size independent) hardness including other hardening mechanisms like precipitation and grain boundary strengthening, and the characteristic length h^* representing the ISE. The dimensionless inverse depth term h^*/h_c is associated with the additional hardening contribution of GNDs populating the dislocation forest. If the experimental data are plotted in terms of H_{IT}^2 vs $1/h_c$, the data follow a straight line according to Eq. (1). Such Nix–Gao (NG) plots are considered below. However, later studies[36,42–44] demonstrated that deviations from linearity are not, or at least not exclusively, caused by experimental issues such as the quality of surface preparation, tip blunting, or pileup. Instead, physical reasons, in particular, a maximum allowable density of GNDs, play a major role at smaller contact depths (highest values of $1/h_c$).[43] Therefore, straight lines were only fitted to the data in the range of the smallest $1/h_c$. The NG plots obtained in the present study are shown in Figs. 7(a)–7(f) for the cases of homogeneous materials: the unirradiated and neutron-irradiated samples of Fe-9Cr and Fe-9Cr-NiSiP. Deviations from linearity are confirmed at higher values of $1/h_c$.

In order to take into account the breakdown of the original NG relation at higher values of $1/h_c$, some authors suggested

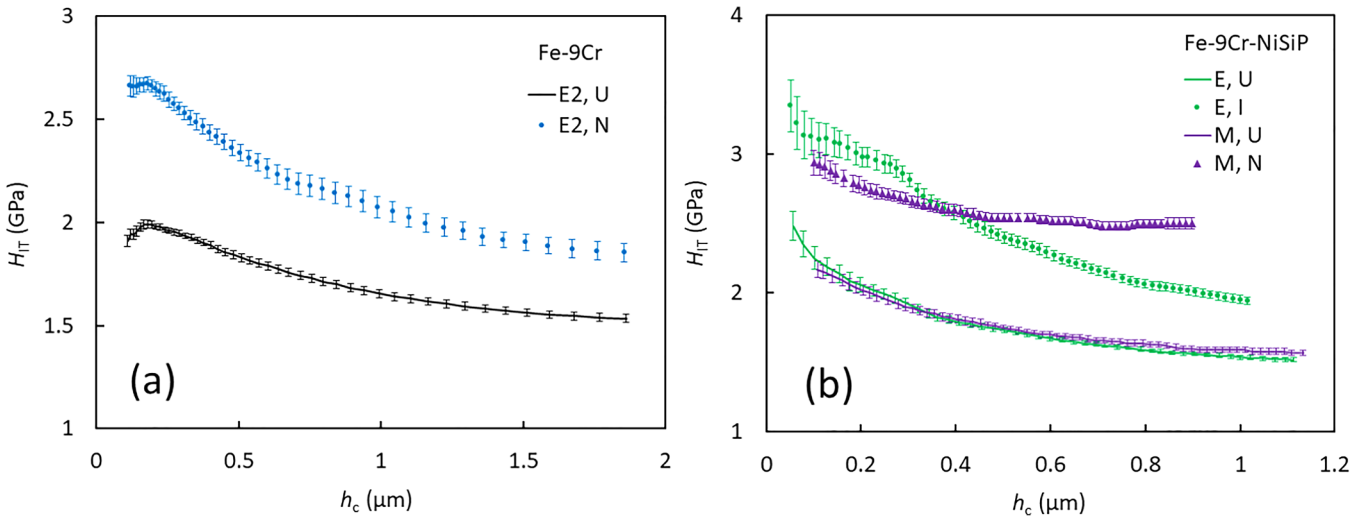

FIG. 6. Results of nanoindentation tests for neutron-irradiated samples and unirradiated references. (a) Fe-9Cr; (b) Fe-9Cr-NiSiP and comparison with the "1 dpa" ion irradiation.

modifications to Eq. (1).[41–44,68] Specifically, it was noted[43] that the GND density under the indenter is not uniformly distributed as assumed in the original work.[28] It rather diverges at the periphery of the contact area requiring regularization by a cut-off in terms of a maximum allowable GND density[43] $\hat{\rho}_{GND}$. Physically speaking, this cut-off can be attributed to the breakdown of the Taylor relation for forest hardening, when spontaneous nucleation of GNDs prevails. Here, we translate $\hat{\rho}_{GND} = 1/(b\bar{h})$ into a cut-off depth $\bar{h}$, with b denoting the length of the Burgers vector, and propose an exponential phase-out of the scaling regime due to that maximum allowable GND density,

$$H_{IT} = H_0\sqrt{1+\frac{h^*}{h_c}\exp\left(-\frac{\bar{h}}{h_c}\right)}. \tag{2}$$

In what follows, we refer to Eq. (2) as the generalized NG relation with respect to Eq. (1). We note that the cut-off depth $\bar{h}$ induces the breakdown of the power-law scaling inherent to the original NG relation. The original NG relation is recovered for $\bar{h} \to 0$. The function in Eq. (2) has a maximum at $h_c = \bar{h}$. The hardness decrease with decreasing $h_c < \bar{h}$ will not be considered below. Fits of Eq. (2) to the data obtained for the homogeneous (unirradiated and neutron-irradiated) cases are included in Fig. 7.

The values of the bulk-equivalent hardness H_0, the characteristic length h^* and the cut-off depth $\bar{h}$ obtained by application of Eqs. (1) and (2) are summarized in Table III. The comparisons of the bulk-equivalent hardness for the unirradiated samples of Fe-9Cr (E vs E2) and Fe-9Cr-NiSiP (E vs M) indicate that systematic errors are of the order of 10% and prevail over statistical errors. Bulk-equivalent hardness values H_0 from the original NG Eq. (1) tend to be larger than those from its generalization Eq. (2), while the opposite is true for the values of the characteristic length h^*.

The Vickers hardness (HV10) values measured for the homogeneous cases (U and N) are listed in Table IV along with their irradiation-induced changes. The respective values of the bulk-equivalent hardness according to Eq. (1) are shown for comparison.

D. Models for the case of ion irradiation

Except for the lowest indentation depths, the volume of the indentation plastic zone in ion-irradiated samples is partly occupied by the irradiated layer and partly by the unirradiated substrate. Therefore, direct fits of either Eq. (1) or (2) to the measured data are questionable. This caveat particularly applies to the original NG model, which assumes the GNDs to be uniformly distributed in a hemispherical dislocation core underneath the indenter contact area. For the generalized NG model proposed here, this is less of a concern, as the GNDs are envisaged to concentrate at the periphery of the contact area,[43] where their density approaches $\hat{\rho}_{GND}$. As a starting point, we approximate the plastic zone as a hemisphere and calculate the composite hardness with weights according to the volume fractions of the plastic zone occupied by the irradiated layer, which is assumed to be homogeneous, and the substrate. This kind of model,[38] referred to as Model A below, was recently reconsidered for ion-irradiated samples.[18,34] The dpa profile is approximated as the average box-like profile plotted in Fig. 1. The model hardness H_A can then be expressed according to Eqs. (3)–(5) as

$$H_A = f_i H_i + (1-f_i)H_u, \tag{3}$$

$$f_i = \begin{cases} 1 & \text{for} \quad x \geq 1, \\ \frac{3}{2}x - \frac{1}{2}x^3 & \text{for} \quad x < 1, \end{cases} \tag{4}$$

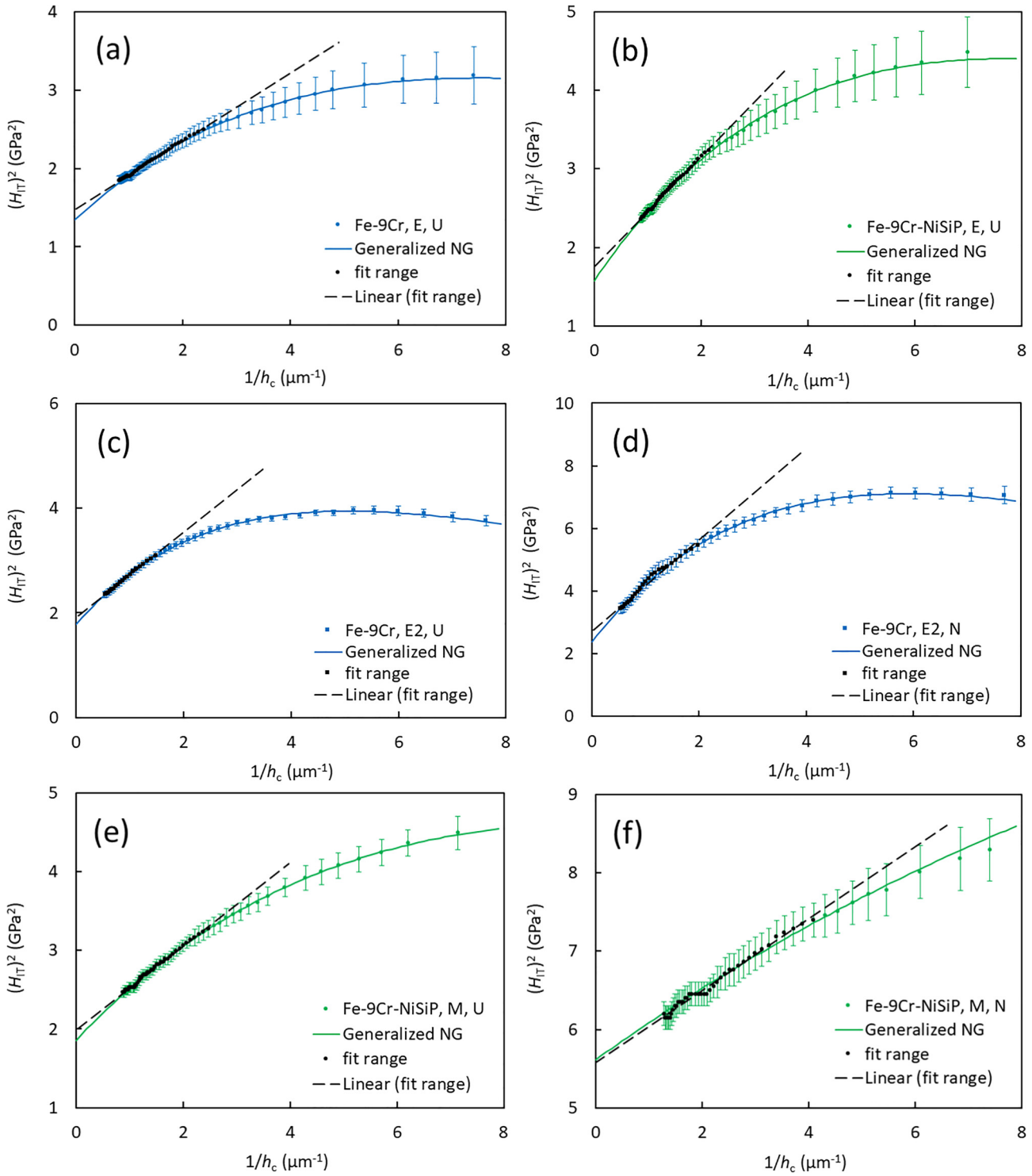

FIG. 7. Original (black dashed lines) and generalized (colored solid lines) Nix–Gao fits of the hardness curves obtained for the homogeneous samples; (a) electrolytically polished unirradiated Fe-9Cr; (b) electrolytically polished unirradiated Fe-9Cr-NiSiP; (c) electrolytically polished (E2) unirradiated Fe-9Cr; (d) electrolytically polished (E2) neutron-irradiated Fe-9Cr; (e) mechanically polished unirradiated Fe-9Cr-NiSiP; (f) mechanically polished neutron-irradiated Fe-9Cr-NiSiP.

TABLE III. Values and errors of the bulk-equivalent hardness and the characteristic lengths h^* derived from the original and generalized Nix–Gao (NG) approaches. Errors of the last digit in parentheses.

	Original NG Eq. (1)			Generalized NG Eq. (2)[a]		
Material/sample	$h_{c,min}$ (μm)	H_0 (GPa)	h^* (μm)	H_0 (GPa)	h^* (μm)	$\bar{h}$ (μm)
Fe-9Cr, E, U	0.42	1.217(3)	0.293(4)	1.158	0.488	0.133
Fe-9Cr, E2, U	0.65	1.379(3)	0.426(6)	1.334	0.655	0.198
Fe-9Cr, E2, N	0.50	1.65(3)	0.52(3)	1.541	0.919	0.170
Fe-9Cr-NiSiP, E, U	0.46	1.323(4)	0.401(6)	1.254	0.638	0.130
Fe-9Cr-NiSiP, M, U	0.41	1.411(4)	0.267(6)	1.363	0.389	0.095
Fe-9Cr-NiSiP, M, N	0.24	2.360(4)	0.083(2)	2.369	0.087	0.032

[a] $h_{c,min} = 0.15\,\mu$m.

$$x = \frac{d_i}{c}\frac{1}{h_c}. \tag{5}$$

In Eq. (3), H_u and H_i are the h_c-dependent indentation hardness values according to either Eq. (1) (Model A1) or Eq. (2) (Model A2) of the unirradiated substrate and the ion-irradiated layer, respectively. The weight factor f_i is the volume fraction of the plastic zone occupied by the irradiated layer. In Eq. (5), $d_i = 1.65\,\mu$m is the effective thickness of the irradiated layer and the radius R of the hemispherical plastic zone is taken as a multiple c of the contact depth h_c. Within Model A1, Eq. (3) with Eq. (1) is fitted to the measured H_{IT}–h_c curves taking $H_{0,u}$ and h^*_u from the original NG fits of the unirradiated reference sample (Table III) as fixed and treating $H_{0,i}$, h^*_i and c as fit parameters. It is important to note that the straight lines for the unirradiated samples in Fig. 7 systematically deviate from the measured curves for indentation depths smaller than 0.4 μm ($1/h_c > 2.5\,\mu\text{m}^{-1}$). Consequentially, the fit range for Model A1 was chosen as $1/h_c < 2.5\,\mu\text{m}^{-1}$. The least-squares fits for the ion-irradiated samples are summarized in Fig. 8. The best-fit parameters for Model A1 are listed in Table V. In the last two lines of Table V, the value of c = 5.6 was taken as fixed to improve comparability with sample Fe-9Cr, E, I. The fit curves for Model A1 asymptotically approach straight lines for $1/h_c \to 0$ (unirradiated substrate) and $1/h_c \to \infty$ (irradiated layer) with a gradual transition. As expected from the design of the model, the curves tend to deviate from the experimental data for $1/h_c > 2.5\,\mu\text{m}^{-1}$.

TABLE IV. Bulk-equivalent hardness (from Table III, original NG) and measured Vickers hardness along with their neutron-irradiation-induced differences. Errors of the last digit in parentheses.

Material/sample	H_0 (GPa)	ΔH_0 (GPa)	HV10	ΔHV10
Fe-9Cr, E2, U	1.38	…	117(2)	…
Fe-9Cr, E2, N	1.65	0.27	139(2)	22(3)
Fe-9Cr-NiSiP, M, U	1.41	…	115(2)	…
Fe-9Cr-NiSiP, M, N	2.36	0.95	187(3)	72(4)

Fits of Model A2, based on Eq. (2) instead of Eq. (1), to the data are shown in Figs. 8(a) and 8(b) for the "1 dpa" ion irradiations of Fe-9Cr and Fe-9Cr-NiSiP (solid lines). The fit range for Model A2 was chosen as $1/h_c < 7\,\mu\text{m}^{-1}$. This wider fit range as compared to the A1 fits was possible because the generalized NG relation Eq. (2) provided good fits for the unirradiated reference samples, which represent the substrate in Model A2, in the same range. In order to reduce the number of free model parameters, the values of the bulk-equivalent hardness H_0, the characteristic length h^*, and the cut-off depth $\bar{h}$ of the unirradiated substrate, which enter into Eq. (3), were taken as fixed (according to the respective values listed in Table III). Moreover, we assumed $\bar{h}_i = \bar{h}_u$. The remaining parameters available for fitting are c, $H_{0,i}$, and h^*_i. The best-fit parameters for Model A2 are compiled in Table V. Figures 8(a) and 8(b) indicate that Model A2 provides good fits within error bars throughout the whole plotted range. In order to retrace the effect of the assumptions related to the application of Model A1 on the fit parameters, we have applied Model A1 in the range $1/h_c < 2.5\,\mu\text{m}^{-1}$ (as before with the experimental data) to the curves obtained for Model A2. The results are also included in Table V. These data are important for the discussion.

The best-fit parameters for Models A1 and A2 listed in Table V are reasonable in several respects. Indeed, the obtained values of c are in the range 5–10 reported for the size of the plastic zone.[23] The best-fit values of $H_{0,i}$ are always larger than the H_0 values of the respective unirradiated reference samples. Moreover, the best-fit values of h^*_i are always smaller than the h^* values of the reference samples. Nevertheless, the comparisons of Models A1 and A2 included in Table V indicate considerable deviations in the absolute values of the fit parameters. This observation is to be addressed in the discussion.

Contrary to Model A, a second model (labeled B1) will explicitly take into account the damage gradient in the irradiated layer while keeping Eq. (1) as starting point.[25,31,32,39,40] According to these models, Eq. (4) has to be replaced by a sum (or integral[31]) over thin slices numbered using the subscript k. f_k is the volume fraction of the hemispherical plastic zone occupied by slice k, which means, a thin segment of a hemisphere,

$$H_B = \sum_k f_k H_k \text{ with } \sum_k f_k = 1. \tag{6}$$

The hardness H_k of slice k is given by Eq. (7),

$$H_k = \begin{cases} (H_{0,u} + aD_k^p)\sqrt{1 + \dfrac{h^*_k}{h_c}} & \text{for} \quad D_k > 0, \\ H_{0,u}\sqrt{1 + \dfrac{h^*_u}{h_c}} & \text{for} \quad D_k = 0, \end{cases} \tag{7}$$

where D_k is the displacement damage in slice k according to the SRIM damage profile (Fig. 1); a and p are pre-factor and exponent assuming the irradiation-induced increase of the hardness to obey a power-law dependence on displacement damage. To simplify the fit

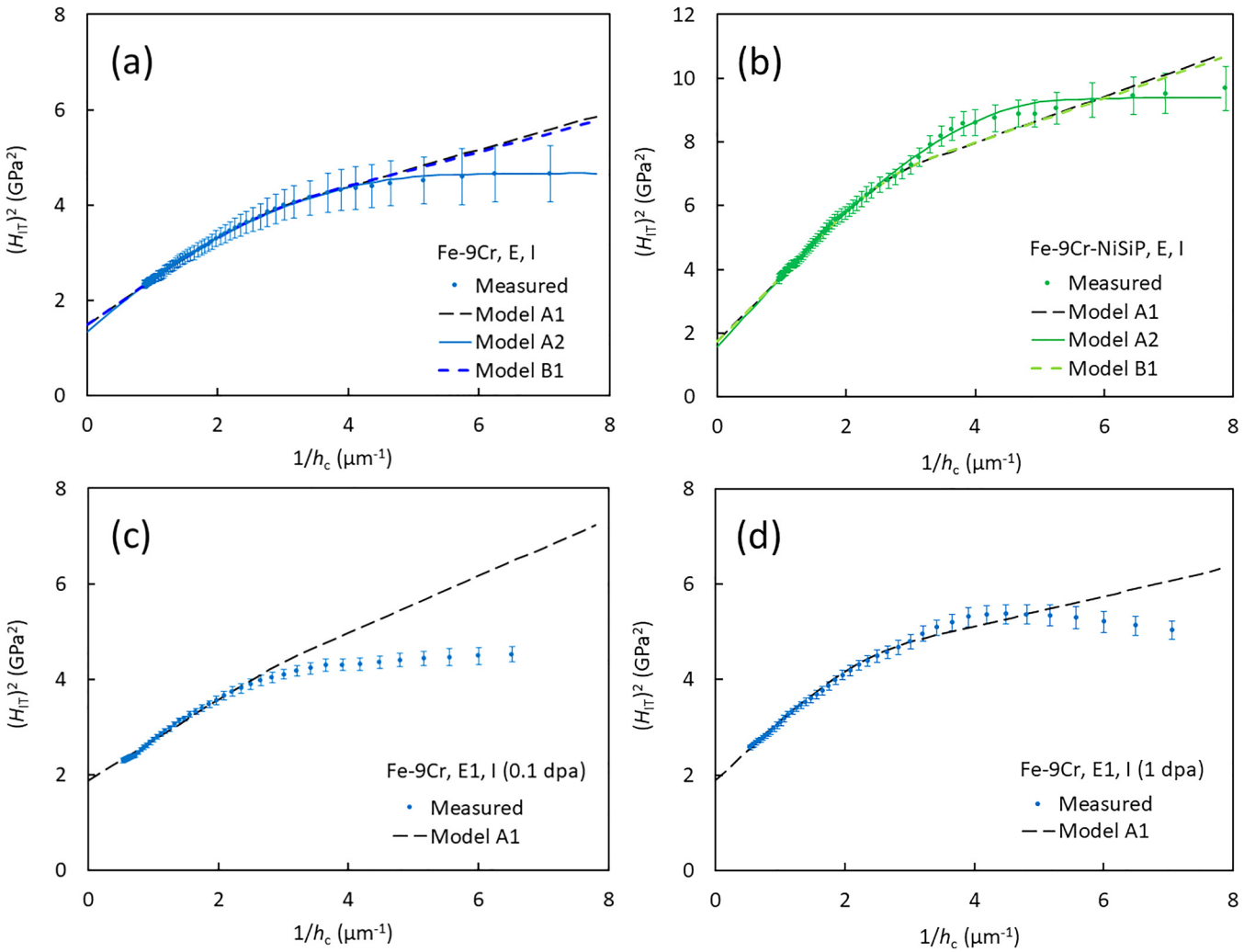

FIG. 8. Model A1 and A2 fit curves for the measurements on the ion-irradiated samples. (a) "1 dpa" irradiation of Fe-9Cr, (b) "1 dpa" irradiation of Fe-9Cr-NiSiP, (c) "0.1 dpa" irradiation of Fe-9Cr (procedure E1), (d) "1 dpa" irradiation of Fe-9Cr (procedure E1). Model B1 in (a) and (b) will be introduced below.

procedure and reduce the number of parameters, $H_{0,u}$ and h_u^* are taken as fixed from the original NG fits of the unirradiated reference samples (see Table III). The range of fit was adopted from case A1. All characteristic lengths h_k^* of the irradiated layers are replaced by their effective value h_i^* obtained before using Model A1. The remaining three fit parameters are c (involved in the f_k terms), a and p. In contrast to the present approach, Röder[31] treated $H_{0,u}$ as a fit parameter. Moreover, these authors did not distinguish between h_u^* and h_i^* and treated h^* as one more fit parameter.

The fit curves derived using Model B1 are included in Figs. 8(a) and 8(b) for ion-irradiated Fe-9Cr and Fe-9Cr-NiSiP, respectively. One notes that the B1 fits do not give rise to major deviations from A1 fits. The benefit is rather the capability to extract the dependence of hardness on displacement damage in terms of a best-fit power-law dependence according to Eq. (7). This is summarized in Fig. 9 and Table VI.

Larger plastic zone size factors c are obtained using Model B1 as compared to Model A1. Most notably, the power-law exponents according to Model B1 are rather small, which gives rise to the flat hardness profiles across the irradiated layer in Fig. 9(b). These flat profiles retrospectively explain why the box-like approximation of the ion-irradiated layer according to Model A1 works rather well and causes only minor deviations from Model B1 in Figs. 8(a) and 8(b). At the same time, this observation underlines the importance of describing the ISE more realistically through the application of the generalization of the NG model (Model A2 vs A1).

TABLE V. Best-fit values of the plastic zone size factor c, the bulk-equivalent hardness, and the characteristic length of the irradiated layer calculated using Model A1 (or Model A2 as specified). Fixed values of $H_{0,u}$, h_u^* (and $\bar{h}$ for Model A2) from Table III.

Material/sample	c	$H_{0,i}$ (GPa)	h_i^* (μm)
Fe-9Cr, E, I ("1 dpa")	5.6	1.68	0.138
Model A2 on same exp. data	9.0	1.97	0.073
Model A1 on curve from A2	4.5	1.55	0.205
Fe-9Cr-NiSiP, E, I ("1 dpa")	5.3	2.25	0.144
Model A2 on same exp. data	8.8	2.82	0.064
Model A1 on curve from A2	6.0	2.35	0.120
Fe-9Cr, E1, I ("0.1 dpa")[a]	5.6	1.60	0.232
Fe-9Cr, E1, I ("1 dpa")[a]	5.6	1.96	0.082

[a]$H_{0,u} = 1.37$ GPa, $h_u^* = 0.273$ μm. Fixed value of c adopted from Fe-9Cr, E, I ("1 dpa").

IV. DISCUSSION

A. Effect of Ni, Si, and P

Figure 5(a) indicates that the addition of Ni, Si, and P gives rise to a slightly higher indentation hardness of unirradiated Fe-9Cr-NiSiP as compared to Fe-9Cr in the whole covered range of contact depth. In terms of the bulk-equivalent hardness derived using Eq. (1), the increase amounts to 8.7%. It is reasonable to assume that this moderate increase is mainly due to the addition of Si,[69] which is known as a solid solution hardener in steel making. Interestingly, the higher bulk-equivalent hardness does not manifest itself in proportional increases of the measured Vickers hardness and yield stress, see Table II. In any case, both unirradiated materials are mechanically similar.

In contrast, the irradiation-induced increase of hardness observed for Fe-9Cr-NiSiP is much larger than for Fe-9Cr.

TABLE VI. Fixed and best-fit parameters for Model B1.

	Fixed parameters			Best-fit parameters		
Material (samples E, I)	$H_{0,u}$ (GPa)	h_u^* (μm)	h_i^* (μm)	c (−)	a (GPa)	p (−)
Fe-9Cr	1.22	0.293	0.138	6.4	0.462	0.10
Fe-9Cr-NiSiP	1.32	0.401	0.144	6.2	0.926	0.04

Neutron irradiation up to 0.11 dpa gives rise to a 20% increase of the bulk hardness of Fe-9Cr derived using Eq. (1) as compared to 67% for Fe-9Cr-NiSiP. These increases are correlated with the measured increase of Vickers hardness as will be discussed later. The higher irradiation-induced hardening observed for the Ni–Si–P-enriched alloy is the result of reported irradiation-induced microstructural changes.[54,55] Indeed, the identification of irradiation-induced Ni–Si–P-rich clusters[70] motivated the fabrication and irradiation of a broader set of alloys that include those of the present study. The dominant microstructural features in neutron-irradiated Fe-9Cr-NiSiP[54] are solute clusters of the mean diameter 2 nm and the number density 7×10^{23} m^{-3}. In Fe-9Cr, Ni–Si–P-rich clusters cannot form because of the scarcity of the constituent elements (cf. Table I). Nanovoids with mean diameter 1.8 nm and number density 4×10^{23} m^{-3} were reported instead.[54] Dislocation loops[55] and α'-phase particles[70] also contribute to the irradiation hardening of both neutron-irradiated alloys. Each of these types of nanofeatures operates as an obstacle for dislocation motion. In essence, the reported microstructures can qualitatively explain the observed differences in neutron-irradiation-induced hardening of Fe-9Cr and Fe-9Cr-NiSiP.

The hardening induced by ion irradiation unfolds a similar picture with some specifics worth mentioning. The microstructure

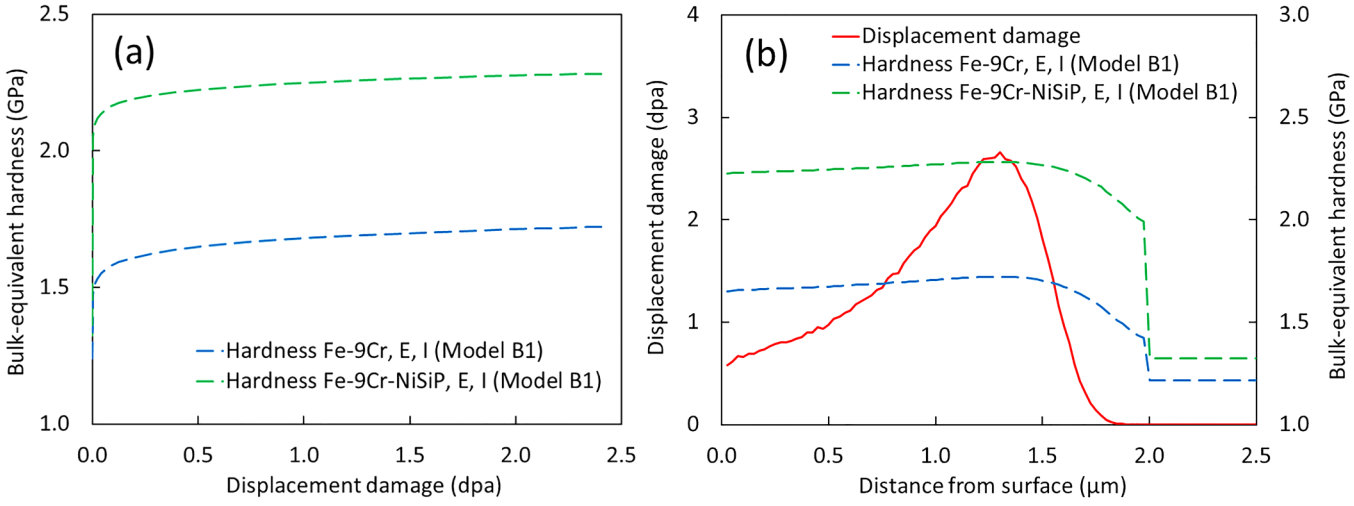

FIG. 9. Best-fit results derived for Model B1 for ion-irradiated Fe-9Cr and Fe-9Cr-NiSiP. (a) Bulk-equivalent hardness as a function of displacement damage; (b) displacement damage (left vertical axis) and bulk-equivalent hardness (right vertical axis) in the ion-irradiated layer as functions of the distance from the irradiated surface.

of the ion-irradiated samples differs from the case of neutron irradiation for two major reasons, namely, the steep damage gradients and the implanted ions. Ni–Si–P-rich clusters were reported to form under ion irradiation as well.[57] However, the formation of α′-phase particles is largely suppressed due to the injected self-interstitial atoms,[4] which also affect the formation of vacancy clusters and loops. A depth-resolved study of the irradiation-induced microstructure in Fe-9Cr (the same material and same ion-irradiation condition as in the present study) identified the dominant type of nanofeatures as dislocation loops.[56] Three distinct regions of depth were identified. The region closest to the irradiated surface (reaching up to 0.8 μm depth), where the concentration of implanted ions can be neglected, exhibited a microstructure resembling the case of neutron irradiation, namely, loops decorating pre-existing line dislocations. In contrast, the microstructure differed from the case of neutron irradiation in the deeper ranges (0.8–1.5 μm depth) affected by the stopped ions. The knowledge of the depth-dependent microstructure allowed a microstructure-informed hardening model to be applied.[61] The predicted hardening was reported to reasonably agree with the measured indentation hardness as a function of contact depth. Unfortunately, the depth-dependent microstructure for ion-irradiated Fe-9Cr-NiSiP alloy is not available. However, the additional formation of Ni–Si–P-enriched clusters under ion irradiation may qualitatively explain the respective observations of the present study, see Fig. 5 and Table V. According to Tables III and V, bulk-equivalent hardness values increase from 1.22 to 1.68 GPa (Model A1, original NG) due to the "1 dpa" ion irradiation of Fe-9Cr, while they increase from 1.32 to 2.25 GPa for Fe-9Cr-NiSiP, meaning by 38% and 70%, respectively.

The characteristic lengths h^* for unirradiated Fe-9Cr and Fe-9Cr-NiSiP are comparable in magnitude and generally decrease as a result of irradiation, with the exception of neutron-irradiated Fe-9Cr, for which h^* was observed to be higher than for the respective unirradiated reference. This is tentatively considered an experimental artifact and requires further attention. The irradiation-induced decrease of h^* tends to be more pronounced for Fe-9Cr-NiSiP. This is understandable on the basis of the higher number density of irradiation-induced nanofeatures, which entails a smaller mean spacing of obstacles for dislocations, hence a smaller characteristic length. The cut-off depth approximately agrees for unirradiated Fe-9Cr and Fe-9Cr-NiSiP. It also exhibits a tendency to decrease as a result of irradiation.

B. Bulk-equivalent hardness and Vickers hardness

Application of the original NG approach based on Eq. (1) allows two parameters, namely, the bulk-equivalent hardness and a characteristic length parameter, to be specified by fitting straight lines to a limited range of data. The linear range in terms of H_{IT}^2 vs $1/h_c$ was found to typically correspond to $h_c > 0.4\,\mu$m. Zhu[36] reported a broader range of linearity corresponding to $h_c > 0.15\,\mu$m. However, reinspection of those authors' plots indicates some curvature even for $h_c > 0.15\,\mu$m, so the deviation from the present study is not dramatic.

Application of the generalized NG approach based on Eq. (2) allows derivation of an additional parameter, which is related to the maximum allowable density of GNDs. The generalized NG relation accounts for curvature, it provides good fits (within experimental errors) for wider ranges of contact depth, at least $h_c > 0.15\,\mu$m in the present study. This is a strong argument in favor of a maximum allowable GND density. However, we cannot claim that the curvature would be exclusively due to this effect. A critical analysis of potential sources of curvature related to the test procedure including surface preparation and pileup correction (see below) demonstrated that proper consideration of these factors did not eliminate the curvature.[36] Zero-point determination has been identified recently[64] to be also critical for curvature, but the good fits obtained here without applying the suggested method of zero-point correction do not allow us to be more specific. It is also important to note that other analytic expressions aimed to overcome the limitations of the original NG approach were suggested.[41–44,68] The reported expressions typically allow the observed curvature to be reproduced over extended ranges of contact depth.[44] A critical discussion of different expressions is, however, beyond the scope of the present study. The benefit of Eq. (2) in the present context is rather the extension of the usable range of contact depth as compared to Eq. (1) in combination with its simplicity and physical plausibility. The extension of the usable range toward smaller contact depths is particularly important in the case of ion-irradiated samples (see below). It allows improving the database used for separating the influence of ISE from spatially limited and strongly graded ion-irradiation-induced hardness increments.

Coming back to the bulk-equivalent hardness, Table III indicates the robustness of the physically weaker original NG approach comparable with the generalized NG approach for homogeneous materials. This is due to the fact that H_0 derives from the extrapolation to large depths h_c, for which the generalization does not matter. For the unirradiated and neutron-irradiated samples, the estimated bulk-equivalent hardness and the measured Vickers hardness are compared in Fig. 10. We have used the same format as Zhu[36] for the sake of better comparability. Moreover, we have added data points from our previous work[24,40] obtained using the same procedures of data analysis (no pileup correction).

Figure 10 demonstrates a strong correlation between bulk-equivalent hardness and Vickers hardness for the alloys of the present study. This finding is consistent with the broader set of alloys covering a wider range of hardness. The regression line indicates a 10% smaller slope as compared to the ideal correlation, the factor of proportionality arising from the use of both the actual (instead of projected) area and the units of kgf/mm^2 (instead of MPa) in the definition of Vickers hardness. The smaller slope is equivalent to a 10% overestimation of the bulk-equivalent hardness. At this point it is interesting to note that a larger overestimation of up to 30% was reported[36] for several Fe–Cr-based data sets including published works[71–73] and own[36] uncorrected data. This overestimation was demonstrated to be mainly due to pileup effects, which means, an upward flow of material at the periphery of the indentations resulting in an increase of the projected contact area. Indeed, pileup corrections made the data points approaching the ideal correlation.[36] As a secondary factor possibly accounting for deviations from the ideal behavior, these authors also brought forward the unbounded density of GNDs in the original NG

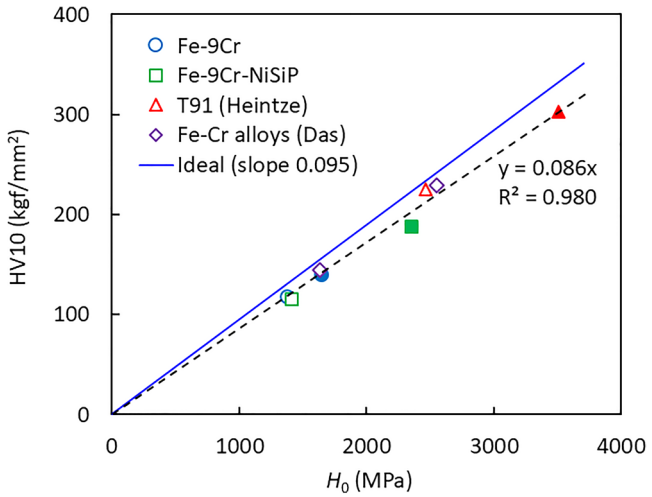

FIG. 10. Comparison of measured Vickers hardness and bulk-equivalent hardness (original NG relation) for the unirradiated (empty symbols) and neutron-irradiated (full symbols) samples of the present study including data reported for the F/M steel T91[24] and for martensitic Fe-9Cr and Eurofer97.[40] The observed empirical correlation and the ideal correlation[36] are indicated.

model. Application of the generalized NG model, assuming a maximum allowed density of GNDs, tends to produce smaller values of the bulk-equivalent hardness according to Table III with the average reduction amounting to 4%. The remaining 6% of overestimation is then concluded to be due to pileup effects, which is consistent with the reported range 5%–14%.[36]

We conclude that it is justified to neglect AFM-based pileup corrections for the purpose of the present study focused on other aspects, while we acknowledge that pileup corrections can further improve the prediction of the bulk-equivalent hardness.

C. Critical discussion of models for ion irradiation

According to Model A,[18,38] the ion-irradiated layer is approximated by a homogeneous layer of uniform thickness on a homogeneous substrate. The hardness-related properties of the system are represented by step-like functions of depth arising from the approximate box-like damage profile, while the elastic properties of layer and substrate agree. Further key assumptions are a hemispherical plastic zone and a composite hardness being the volume-weighted average of the hardness of layer and substrate. "Volume-weighted" refers to the volume fractions of the plastic zone occupied by the layer and the substrate. The layer hardness as well as the substrate hardness can be expressed according to either Eq. (1) (Model A1) or Eq. (2) (Model A2). Knowing the measured hardness of the layer-substrate system and the hardness of the unirradiated reference measured beforehand, the hardness of the layer can be recovered in terms of the parameters of the underlying equation by fitting the model to the experiment. The best-fit values of the plastic zone size factor, the bulk-equivalent hardness of the layer, and the characteristic length of the layer obtained for Model A1 (Fig. 11) indicate that

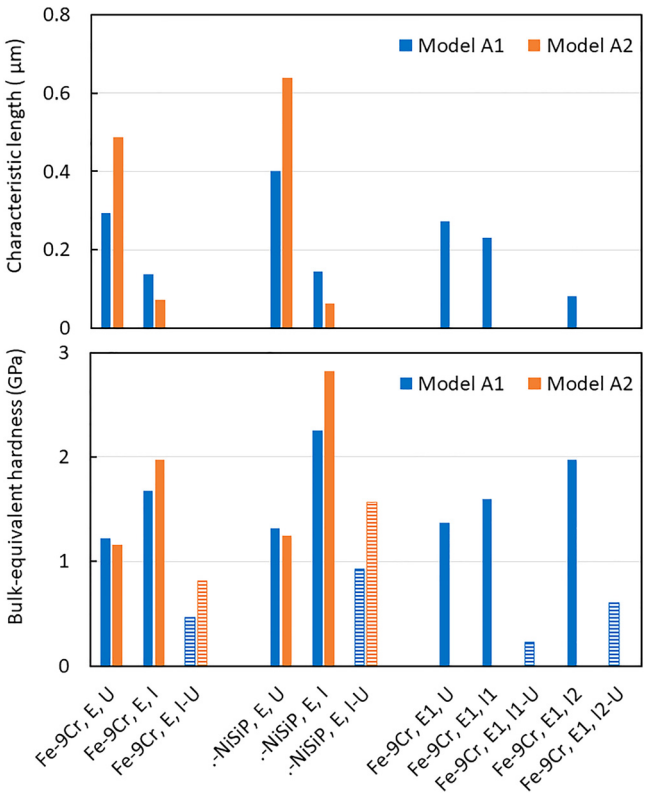

FIG. 11. Comparisons of the characteristic length and the bulk-equivalent hardness of the ion-irradiated layers (I) obtained using Models A1 and A2. The unirradiated references (U) (i.e., the substrate properties) and the irradiation-induced differences (I-U, hatched bars) are also plotted. I1 and I2 refer to the "0.1 dpa" and "1 dpa" irradiations, respectively.

- The best-fit radius of the plastic zone is five to six times the contact depth, which is included in the reasonable range.[23] Higher hardening (Fe-9Cr-NiSiP) gives rise to a smaller plastic zone than lower hardening (Fe-9Cr). This is consistent with the prediction from the expanding cavity model.[74]
- The best-fit bulk-equivalent hardness of the ion-irradiated layer is always larger than the bulk-equivalent hardness of the unirradiated reference (Fig. 11, blue bars). The corresponding increase is larger for Fe-9Cr-NiSiP as compared to Fe-9Cr. It is also larger for the "1 dpa" irradiation of Fe-9Cr (I2 in Fig. 11) as compared to the "0.1 dpa" irradiation (I1).
- The best-fit value of the characteristic length of the ion-irradiated layer is always smaller than the characteristic length of the unirradiated reference (Fig. 11). This reduction is larger for Fe-9Cr-NiSiP as compared to Fe-9Cr ("1 dpa" irradiations). It is also larger for the "1 dpa" irradiation of Fe-9Cr as compared to the "0.1 dpa" irradiation.

The listed findings are all reasonable with a view to the available microstructural and metallurgical information. However, we

do not possess a criterion capable of validating the model in quantitative terms.

Corresponding results obtained using Model A2 are also included in Fig. 11 (orange bars). These results can be summarized as follows:

- The best-fit radius of the plastic zone is eight to nine times the contact depth. This is significantly larger than for Model A1 but still in the reasonable range.
- As before, the best-fit bulk-equivalent hardness of the ion-irradiated layer is always larger than the bulk hardness of the unirradiated reference (Fig. 11, orange bars). The corresponding increase is larger for Fe-9Cr-NiSiP than for Fe-9Cr ("1 dpa" irradiations). In both cases, the bulk-equivalent hardness of the irradiated layer and its increase are larger than for Model A1.
- While the characteristic length of the substrate is larger than for Model A1, the characteristic length of the irradiated layer is smaller indicating a more pronounced irradiation-induced reduction of h^*.

The set of results obtained using Model A2 is essentially consistent. There are significant differences between the "predictions" of Models A1 and A2. Of course, the wider range of contact depth showing a good fit with the experimental data and the more realistic asymptotic behavior of the density of GNDs are arguments in favor of Model A2. Moreover, the application of Model A1 (range $1/h_c < 2.5\,\mu m^{-1}$) to the fit curves derived from Model A2 roughly reproduces the deviations between the results obtained by direct application of A1 and A2 to the experimental data (Table V). This suggests that the deviations are artifacts caused by the physical limitations of Model A1. Tentatively, we should perceive Model A2 as a reference and Model A1 as inferior due to physical limitations. In any case, a comparison with the results obtained for neutron-irradiated materials will be useful.

As already demonstrated in the results section, Model B1, by explicitly taking into account the damage profile,[31] basically allows the bulk-equivalent hardness to be recovered as a function of displacement damage (Fig. 9). However, the range of contact depth for which a good fit is observed is not much wider than for Model A1. A possible combination of Model B with Eq. (2) and its numerical implementation, on the other hand, requires future attention.

D. Ion irradiation vs neutron irradiation

For reference, the results obtained for the available neutron-irradiated samples of Fe-9Cr and Fe-9Cr-NiSiP are plotted in Fig. 12 (full symbols) in terms of the increase of bulk hardness vs displacement damage. The upper one of each pair of data points is related to the application of the original NG relation, Eq. (1), while the lower one refers to the generalized NG relation, Eq. (2). The correlation with Vickers hardness was already considered in Sec. IV B. As mentioned before, the generalized NG relation yields results closer to the ideal correlation between bulk and Vickers hardness. The results obtained for ion-irradiated samples are plotted as open symbols (Models A1 and A2) and dashed lines (Model B1). In order to evaluate differences between materials, models, and irradiations, we should not just take the statistical errors as a basis (see Figs. 3–8 and Table III) but also account for

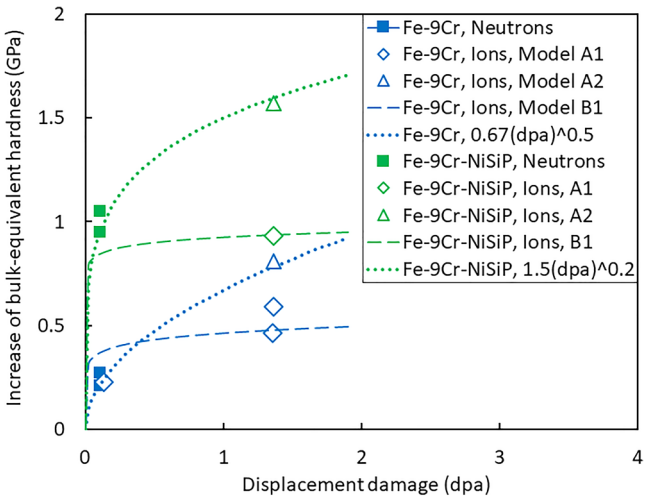

FIG. 12. Summary of results on the irradiation-induced increase of the bulk-equivalent hardness obtained using Eqs. (1) and (2) for neutrons and Models A1, A2, and B1 for ions.

typical scatter between different laboratories and different surface preparation procedures [see, for example, Figs. 3(b) and 10].

Application of Models A1 and B1 to ion-irradiated Fe-9Cr-NiSiP indicates a smaller irradiation-induced increase in the bulk-equivalent hardness in the range from 1 to 2 dpa as compared to the increase of the bulk hardness for the neutron irradiation up to 0.11 dpa. This is not reasonable and provides one more argument in favor of Model A2. Empirical power-law functions representing the data for neutron-irradiated and ion-irradiated samples using Eq. (2) and Model A2, respectively, have, therefore, been added to the plot (dotted lines). The empirical exponents are 0.5 for Fe-9Cr and 0.2 for Fe-9Cr-NiSiP. Both are in the range of reported exponents.[75] Instead, the power-law exponents obtained directly by applying Model B1 (see Table VI) appear to be unreasonably small.

None of the models applied to ion-irradiated samples takes into account the effect of the implanted ions. Little attention has been paid to this issue in the reported nanoindentation studies. It was demonstrated[40] that the effect of implanted ions is a secondary factor as compared to the effect of displacement damage in the considered cases. This does not mean that the effect of implanted ions would be generally negligible. Irradiations with self-ions of sufficiently high energy, 5 MeV being a minimum for Fe-based alloys,[3,36] extend the region of vanishing concentration of implanted ions (safe zone) toward larger depths. Indeed, the irradiated microstructure in the safe zone of Fe-9Cr irradiated with 5 MeV iron ions was found to resemble the microstructure of the neutron-irradiated counterpart, while this is not the case in the stopping range of ions.[56] It would therefore be useful to raise the ion energy and simultaneously reduce the maximum contact depth for analysis. For the latter, the application of Eq. (2) instead of Eq. (1) is essential as demonstrated above. However, a systematic study on how much the upper bound of the range of contact depth

used for fitting Model A2 to the experimental data can be reduced remains to be done.

V. CONCLUSIONS

The irradiation-induced hardening observed for Fe-9Cr and Fe-9Cr-NiSiP as characterized by nanoindentation is qualitatively well understood in terms of the reported irradiated microstructures. While the unirradiated hardness is comparable for both materials, the addition of Ni, Si, and P gives rise to an increase in the amount of irradiation hardening for both neutrons and ions. Quantitative microstructure-informed prediction of hardening is beyond the scope of the present study.

The graded damage structure and localized hardening due to ion irradiation strongly interfere with the indentation size effect (ISE), which can be attributed to the additional forest hardening by geometrically necessary dislocations. Application of the original Nix–Gao approach to the homogeneous cases (i.e., unirradiated and neutron-irradiated samples) gives rise to an overestimation of the bulk-equivalent hardness as compared to the ideal correlation between bulk-equivalent hardness and Vickers hardness. This overestimation splits into parts arising from pileup effects and the unbounded GND density. Application of the generalized Nix–Gao approach, which takes into account a maximum allowable GND density, reduces the overestimation from 10% to 6% in the present case. Moreover, the generalized Nix–Gao approach allows the experimental data to be fit in much wider ranges of contact depth.

For the ion-irradiated samples, a first model approximates the irradiated region as a homogeneous layer on the unirradiated substrate. A composite hardness is calculated as the weighted average of layer and substrate hardness taking the volume fractions of the hemispherical plastic zone occupied by layer and substrate as weights. The combination of this model with the original Nix–Gao approach provides fits of the experimental data in limited ranges of contact depth. The resulting estimates of the plastic zone size, bulk-equivalent hardness, and characteristic length of the irradiated layers are reasonable.

The combination of the same model with the generalized Nix–Gao approach is superior in a number of respects including fits of the experimental data in wider ranges of contact depth and better consistency of the bulk-equivalent hardness with the results derived for neutron-irradiated samples.

A second model approximating hardening as a power-law function of displacement damage allows, in principle, best-fit values of the pre-factor and exponent to be derived. This was tentatively demonstrated in combination with the original Nix–Gao approach. However, the second model was not found to outperform the first model with respect to the quality/range of fitting.

In essence, the combination of a homogeneous irradiated layer with the generalized Nix–Gao model (i.e., Model A2) is tentatively considered the first choice. The superiority of Model A2 resides in its more realistic capturing of hardness and irradiation-induced hardness changes at small indentation depths, which are relevant for ion-irradiated materials. In doing so, Model A2 is more sensitive in accounting for the ISE and its interference with the graded ion-irradiation hardening. Future work will have to address the question of whether or not the upper bound of the fit range in terms of contact depth can be sufficiently reduced in order to prevent the plastic zone from reaching into the influence zone of the implanted ions.

ACKNOWLEDGMENTS

The work reported here received funding from the European Commission within the project M4F (Grant Agreement No. 755039). This work contributes to the Joint Programme on Nuclear Materials (JPNM) within the European Energy Research Alliance (EERA). All ion irradiations were performed at the Ion Beam Center at Helmholtz-Zentrum Dresden-Rossendorf (HZDR). We would like to thank Shavkat Akhmadaliev for assistance with the ion irradiations. Neutron irradiation was performed at the BR2 materials testing reactor of SCK·CEN. Many thanks to Milan Konstantinović for the supply of samples.

AUTHOR DECLARATIONS

Conflict of Interest

The authors have no conflicts to disclose.

Author Contributions

Frank Bergner: Conceptualization (equal); Data curation (equal); Formal analysis (equal); Funding acquisition (equal); Investigation (equal); Methodology (equal); Project administration (equal); Resources (equal); Writing – original draft (lead); Writing – review and editing (lead). **Cornelia Kaden:** Funding acquisition (equal); Investigation (equal); Methodology (equal); Resources (equal); Writing – original draft (supporting); Writing – review and editing (supporting). **Aniruddh Das:** Investigation (equal); Methodology (equal); Writing – original draft (supporting); Writing – review and editing (supporting). **Susana Merino:** Data curation (equal); Formal analysis (equal); Investigation (equal); Methodology (equal); Resources (equal); Writing – original draft (supporting); Writing – review and editing (supporting). **Gonzalo Diego:** Data curation (equal); Formal analysis (equal); Investigation (equal); Methodology (equal); Resources (equal); Writing – original draft (supporting); Writing – review and editing (supporting). **Peter Hähner:** Conceptualization (equal); Data curation (equal); Formal analysis (equal); Funding acquisition (equal); Investigation (equal); Methodology (equal); Project administration (lead); Resources (equal); Writing – original draft (equal); Writing – review and editing (equal).

DATA AVAILABILITY

The data that support the findings of this study are available within the article and from the corresponding author upon reasonable request.

REFERENCES

[1]R. S. Nelson, D. J. Mazey, and J. A. Hudson, J. Nucl. Mater. **37**, 1 (1970).
[2]G. S. Was and S. J. Zinkle, *Comprehensive Nuclear Materials* (Elsevier, 2020), pp. 468–484.
[3]S. J. Zinkle and L. L. Snead, Scr. Mater. **143**, 154 (2018).
[4]O. Tissot, C. Pareige, E. Meslin, B. Décamps, and J. Henry, Mater. Res. Lett. **5**, 117 (2017).

[5]K. Ma, B. Décamps, A. Fraczkiewicz, T. Jourdan, F. Prima, and M. Loyer-Prost, Acta Mater. **212**, 116874 (2021).
[6]E. R. Reese, N. Almirall, T. Yamamoto, S. Tumey, G. Robert Odette, and E. A. Marquis, Scr. Mater. **146**, 213 (2018).
[7]J. G. Gigax, E. Aydogan, T. Chen, D. Chen, L. Shao, Y. Wu, W. Y. Lo, Y. Yang, and F. A. Garner, J. Nucl. Mater. **465**, 343 (2015).
[8]E. Getto, Z. Jiao, A. M. Monterrosa, K. Sun, and G. S. Was, J. Nucl. Mater. **465**, 116 (2015).
[9]C.-L. Ren, Y. Yang, Y.-G. Li, P. Huai, Z.-Y. Zhu, and J. Li, Npj Comput. Mater. **6**, 189 (2020).
[10]G. S. Was, S. Taller, Z. Jiao, A. M. Monterrosa, D. Woodley, D. Jennings, T. Kubley, F. Naab, O. Toader, and E. Uberseder, Nucl. Instrum. Methods Phys. Res., Sect. B **412**, 58 (2017).
[11]J. G. Gigax, H. Kim, E. Aydogan, F. A. Garner, S. Maloy, and L. Shao, Mater. Res. Lett. **5**, 478 (2017).
[12]W. C. Oliver and G. M. Pharr, J. Mater. Res. **7**, 1564 (1992).
[13]T. Chudoba and N. M. Jennett, J. Phys. D: Appl. Phys. **41**, 215407 (2008).
[14]N.N., Standard ISO 14577-1, Metallic materials—Instrumented indentation test for hardness and materials parameters—Part 1 Test method, 2015.
[15]S. J. Zinkle and W. C. Oliver, J. Nucl. Mater. **141–143**, 548 (1986).
[16]C. Robertson, S. Poissonnet, and L. Boulanger, J. Mater. Res. **13**, 2123 (1998).
[17]R. Kasada, Y. Takayama, K. Yabuuchi, and A. Kimura, Fusion Eng. Des. **86**, 2658 (2011).
[18]G. Bonny, T. Khvan, A. Bakaeva, C. Yin, A. Dubinko, C. Cabet, M. Loyer-Prost, N. Castin, A. Bakaev, and D. Terentyev, J. Nucl. Mater. **543**, 152543 (2021).
[19]X. Chen, W. Zhou, X. Zhang, Q. Feng, J. Zheng, X. Liu, B. Tang, J. Li, J. Xue, and S. Peng, J. Appl. Phys. **123**, 025104 (2018).
[20]C. Robertson, B. K. Panigrahi, S. Balaji, S. Kataria, Y. Serruys, M.-H. Mathon, and C. S. Sundar, J. Nucl. Mater. **426**, 240 (2012).
[21]C. D. Hardie and S. G. Roberts, J. Nucl. Mater. **433**, 174 (2013).
[22]Y. Takayama, R. Kasada, Y. Sakamoto, K. Yabuuchi, A. Kimura, M. Ando, D. Hamaguchi, and H. Tanigawa, J. Nucl. Mater. **442**, S23 (2013).
[23]C. K. Dolph, D. J. da Silva, M. J. Swenson, and J. P. Wharry, J. Nucl. Mater. **481**, 33 (2016).
[24]C. Heintze, F. Bergner, S. Akhmadaliev, and E. Altstadt, J. Nucl. Mater. **472**, 196 (2016).
[25]A. Kareer, A. Prasitthipayong, D. Krumwiede, D. M. Collins, P. Hosemann, and S. G. Roberts, J. Nucl. Mater. **498**, 274 (2018).
[26]H. H. Jin, C. S. Shin, and W. W. Kim, Solid State Phenom. **135**, 119 (2008).
[27]S. Agarwal, M. Butterling, M. O. Liedke, K. H. Yano, D. K. Schreiber, A. C. L. Jones, B. P. Uberuaga, Y. Q. Wang, M. Chancey, H. Kim, B. K. Derby, N. Li, D. J. Edwards, P. Hosemann, D. Kaoumi, E. Hirschmann, A. Wagner, and F. A. Selim, J. Appl. Phys. **131**, 125903 (2022).
[28]W. D. Nix and H. Gao, J. Mech. Phys. Solids **46**, 411 (1998).
[29]G. M. Pharr, E. G. Herbert, and Y. Gao, Annu. Rev. Mater. Res. **40**, 271 (2010).
[30]R. Kasada, S. Konishi, K. Yabuuchi, S. Nogami, M. Ando, D. Hamaguchi, and H. Tanigawa, Fusion Eng. Des. **89**, 1637 (2014).
[31]F. Röder, C. Heintze, S. Pecko, S. Akhmadaliev, F. Bergner, A. Ulbricht, and E. Altstadt, Philos. Mag. **98**, 911 (2018).
[32]M. Saleh, Z. Zaidi, M. Ionescu, C. Hurt, K. Short, J. Daniels, P. Munroe, L. Edwards, and D. Bhattacharyya, Int. J. Plast. **86**, 151 (2016).
[33]D. Kiener, A. M. Minor, O. Anderoglu, Y. Wang, S. A. Maloy, and P. Hosemann, J. Mater. Res. **27**, 2724 (2012).
[34]P. Hosemann, D. Kiener, Y. Wang, and S. A. Maloy, J. Nucl. Mater. **425**, 136 (2012).
[35]P. Haušild, J. Nucl. Mater. **551**, 152987 (2021).
[36]P. Zhu, Y. Zhao, S. Agarwal, J. Henry, and S. J. Zinkle, Mater. Des. **213**, 110317 (2022).
[37]X. Xiao and L. Yu, Nucl. Mater. Energy **22**, 100721 (2020).
[38]P. M. Sargent, "Factors affecting the microhardness of solids," Ph.D. thesis (University of Cambridge, UK, 1979).
[39]X. Xiao, Q. Chen, H. Yang, H. Duan, and J. Qu, J. Nucl. Mater. **485**, 80 (2017).
[40]A. Das, E. Altstadt, C. Kaden, G. Kapoor, S. Akhmadaliev, and F. Bergner, Front. Mater. **8**, 811851 (2022).
[41]G. Feng and W. D. Nix, Scr. Mater. **51**, 599 (2004).
[42]Y. Huang, F. Zhang, K. Hwang, W. Nix, G. Pharr, and G. Feng, J. Mech. Phys. Solids **54**, 1668 (2006).
[43]A. Ruiz-Moreno and P. Hähner, Mater. Des. **145**, 168 (2018).
[44]P. Haušild, Philos. Mag. **101**, 420 (2021).
[45]M. A. Mattucci, I. Cherubin, P. Changizian, T. Skippon, and M. R. Daymond, Acta Mater. **207**, 116702 (2021).
[46]H.-S. Kim, D.-H. Lee, M.-Y. Seok, Y. Zhao, W.-J. Kim, D. Kwon, H.-H. Jin, J. Kwon, and J. Jang, J. Nucl. Mater. **487**, 343 (2017).
[47]X. Xiao and L. Yu, J. Nucl. Mater. **503**, 110 (2018).
[48]J. F. Ziegler, M. D. Ziegler, and J. P. Biersack, Nucl. Instrum. Methods Phys. Res., Sect. B **268**, 1818 (2010).
[49]C. D. Hardie, G. R. Odette, Y. Wu, S. Akhmadaliev, and S. G. Roberts, J. Nucl. Mater. **482**, 236 (2016).
[50]D. L. Krumwiede, T. Yamamoto, T. A. Saleh, S. A. Maloy, G. R. Odette, and P. Hosemann, J. Nucl. Mater. **504**, 135 (2018).
[51]K. Kese, P. A. T. Olsson, A.-M. Alvarez Holston, and E. Broitman, J. Nucl. Mater. **487**, 113 (2017).
[52]M. J. Swenson, C. K. Dolph, and J. P. Wharry, J. Nucl. Mater. **479**, 426 (2016).
[53]J. Thomas, F. Teng, D. Murray, and M. A. Okuniewski, MRS Adv. **6**, 1048 (2021).
[54]M. J. Konstantinović, A. Ulbricht, T. Brodziansky, N. Castin, and L. Malerba, J. Nucl. Mater. **540**, 152341 (2020).
[55]A. Dubinko, N. Castin, D. Terentyev, G. Bonny, and M. J. Konstantinović, J. Nucl. Mater. **540**, 152395 (2020).
[56]K. Vogel, P. Chekhonin, C. Kaden, M. Hernández-Mayoral, S. Akhmadaliev, and F. Bergner, Nucl. Mater. Energy **27**, 101007 (2021).
[57]C. Pareige, V. Kuksenko, and P. Pareige, J. Nucl. Mater. **456**, 471 (2015).
[58]L. Malerba, M. J. Caturla, E. Gaganidze, C. Kaden, M. J. Konstantinović, P. Olsson, C. Robertson, D. Rodney, A. M. Ruiz-Moreno, M. Serrano, J. Aktaa, N. Anento, S. Austin, A. Bakaev, J. P. Balbuena, F. Bergner, F. Boioli, M. Boleininger, G. Bonny, N. Castin, J. B. J. Chapman, P. Chekhonin, M. Clozel, B. Devincre, L. Dupuy, G. Diego, S. L. Dudarev, C.-C. Fu, R. Gatti, L. Gélébart, B. Gómez-Ferrer, D. Gonçalves, C. Guerrero, P. M. Gueye, P. Hähner, S. P. Hannula, Q. Hayat, M. Hernández-Mayoral, J. Jagielski, N. Jennett, F. Jiménez, G. Kapoor, A. Kraych, T. Khvan, L. Kurpaska, A. Kuronen, N. Kvashin, O. Libera, P.-W. Ma, T. Manninen, M.-C. Marinica, S. Merino, E. Meslin, F. Mompiou, F. Mota, H. Namburi, C. J. Ortiz, C. Pareige, M. Prester, R. R. Rajakrishnan, M. Sauzay, A. Serra, I. Simonovski, F. Soisson, P. Spätig, D. Tanguy, D. Terentyev, M. Trebala, M. Trochet, A. Ulbricht, M. Vallet, K. Vogel, T. Yalcinkaya, and J. Zhao, Nucl. Mater. Energy **29**, 101051 (2021).
[59]M. J. Konstantinović and L. Malerba, J. Nucl. Mater. **528**, 151879 (2020).
[60]A. Ruiz-Moreno, P. Hähner, L. Kurpaska, J. Jagielski, P. Spätig, M. Trebala, S.-P. Hannula, S. Merino, G. de Diego, H. Namburi, O. Libera, D. Terentyev, T. Khvan, C. Heintze, and N. Jennett, Nanomaterials **10**, 130 (2020).
[61]G. Kapoor, P. Chekhonin, C. Kaden, K. Vogel, and F. Bergner, Nucl. Mater. Energy **30**, 101105 (2022).
[62]F. Bergner, P. Hähner, A. M. Ruiz-Moreno, L. Kurpaska, O. Libera, S. Merino, and G. Diego, Deliverable 6.5, Project M4F, H2020 Euratom WP 2014-2018, 2021.
[63]R. E. Stoller, M. B. Toloczko, G. S. Was, A. G. Certain, S. Dwaraknath, and F. A. Garner, Nucl. Instrum. Methods Phys. Res., Sect. B **310**, 75 (2013).
[64]D. Geng, H. Yu, Y. Okuno, S. Kondo, and R. Kasada, Sci. Rep. **12**, 6391 (2022).
[65]C. Saringer, M. Tkadletz, M. Kratzer, and M. J. Cordill, J. Mater. Res. **36**, 2154 (2021).
[66]C. D. Hardie, S. G. Roberts, and A. J. Bushby, J. Nucl. Mater. **462**, 391 (2015).

[67]T. Chudoba, D. Schwenk, P. Reinstädt, and M. Griepentrog, JOM **74**, 2179 (2022).
[68]J. Wang, T. Volz, S. M. Weygand, and R. Schwaiger, J. Mater. Res. **36**, 2166 (2021).
[69]A. Chauhan, F. Bergner, A. Etienne, J. Aktaa, Y. de Carlan, C. Heintze, D. Litvinov, M. Hernandez-Mayoral, E. Oñorbe, B. Radiguet, and A. Ulbricht, J. Nucl. Mater. **495**, 6 (2017).
[70]V. Kuksenko, C. Pareige, and P. Pareige, J. Nucl. Mater. **432**, 160 (2013).
[71]Y. Yang, C. Zhang, Z. Ding, C. Su, T. Yan, Y. Song, and Y. Cheng, J. Nucl. Mater. **498**, 129 (2018).
[72]K. Yabuuchi, Y. Kuribayashi, S. Nogami, R. Kasada, and A. Hasegawa, J. Nucl. Mater. **446**, 142 (2014).
[73]S. Chen, Y. Miyahara, A. Nomoto, and K. Nishida, Acta Mater. **179**, 61 (2019).
[74]K. L. Johnson, J. Mech. Phys. Solids **18**, 115 (1970).
[75]T. S. Byun and K. Farrell, J. Nucl. Mater. **326**, 86 (2004).